DOI 10.1007/s11223-018-0028-0
Strength of Materials, Vol. 50, No. 5, September, 2018

SHEAR STRENGTH OPTIMIZATION OF LASER-JOINED POLYPHENYLENE SULFIDE-BASED CFRTP AND STAINLESS STEEL

L. Y. Sheng,[a,1] F. Y. Wang,[b] Q. Wang,[b] and J. K. Jiao[b,2]

UDC 539.4

A thermosetting plastic and stainless steel were joined by the fiber laser with and without polyphenylene sulfide (PPS) additive. Its microstructure, interface morphology, and shear strength were investigated. The laser joining is shown to change the microstructure of the stainless steel and result in the heat-affected zone and fusion zone, which contains the lathy ferrite and skeletal ferrite, respectively. Without the PPS interlayer, the additive in the plastic can be overheated and decomposed during laser joining, which is detrimental to the interface bonding. The additive can contribute to the plastic and stainless steel interpenetration, but its amount should be controlled. Insufficient additive quantities cannot fill the gap between stainless steel and plastic, but its higher quantities can cause excessive melting, which would prevent from gaining the joint with optimum shear strength. The appropriate interlayer thickness is 300 μm, which improves the shear strength of the stainless steel and plastic joint to 15.1 MPa.

Keywords: carbon-fiber-reinforced thermosetting plastic, stainless steel, laser joining, polyphenylene sulfide, shear strength.

Introduction. Carbon fiber reinforced thermal polymer (CFRTP) is one of the essential materials for structural applications, especially in space/aircraft industries because of its high strength to weight ratio [1]. However, in most applications, CFRTP always has to join with metal frames to form complete structures, which plays a vital role in hybrid design. Now, the common joining methods between the CFRTP and metal include the mechanical joining, the adhesive bonding and the thermal joining [2]. The mechanical joining technology has advantages of high joint strength and short-time processing, but it has some drawbacks such as stress concentration and fiber damage [3]. The adhesive bonding technology has a good fatigue life, low stress concentration, and corrosion resistance, however, it has some weaknesses such as long curing time and poor environmental tolerance [4]. The thermal joining method has better environmental adaptability compared with the adhesion bonding method and has a more uniform stress distribution compared with the mechanical joining. Therefore, the thermal joining has been considered the most suitable technology for the joining of CFRTP and metal. Thermal joining methods include friction welding [5], laser transmission welding [6], direct laser welding, etc. Among the methods, the laser direct laser joining has attracted more attention, due to its advantages such as high-efficiency, non-contacting, low thermal effect and suitable for opaque CFRTP.

Katayama and Kawahito [7] exhibited that the direct laser irradiates on stainless steel could generate a Cr_2O_3 transition layer on the interface of plastic/stainless steel. Moreover, the research of Tan et al. [8] revealed that the

[a]Shenzhen Institute, Peking University, Shenzhen, China ([1]lysheng@yeah.net). [b]Ningbo Institute of Materials Technology and Engineering, Chinese Academy of Sciences, Ningbo, China ([2]jiaojunke@nimte.ac.cn). Translated from Problemy Prochnosti, No. 5, pp. 153 – 160, September – October, 2018. Original article submitted March 5, 2018.

 0039–2316/18/5005–0824 © 2018 Springer Science+Business Media, LLC

TABLE 1. The Chemical Composition of 304 Stainless Steel (wt.%)

C	Mn	Si	Ni	Cr	S	P	Fe
0.07	0.78	0.56	8.10	18.33	0.006	0.032	Bal.

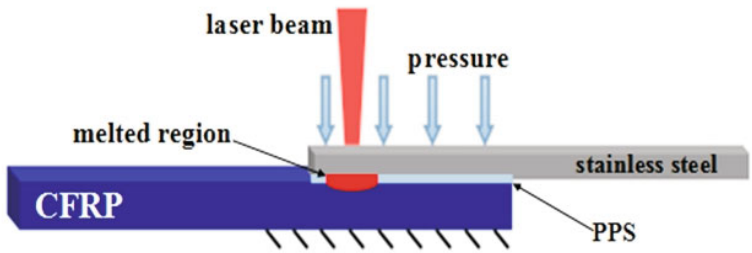

Fig. 1. The schematic diagram of stainless steel and CFRTP laser joint.

existence of Cr layer on the steel surface enhanced the shear strength of the CFRP/steel joint by the Cr-O-PA6T bonding along joint interface. Roesner et al. [9] demonstrated that the machined micro-grooves on the metal surface increased the strength of laser joining plastic/aluminum joint to 24 MPa. Whatever the changing of processing parameter, surface morphology, and surface modification, air bubbles are inevitably generated in the CFRTP. The study of Tan et al. [10] demonstrated that the heat from the laser would result in rapid temperature increases, which could generate the CO_2, NH_3, and H_2O in the CFRP and promote the air bubbles and porosity. Except for the investigation on the laser joining of the CFRTP and metal, the development of the laser technology also encourages the application of laser joining of CFRTP and metal [11]. Recently, we have joined the CFRTP and steel by the fiber laser, and it exhibited relative good processibility [12]. Though the fiber laser could be applied in the joining of CFRTP and metals, there are still many aspects that need to be investigated and clarified, including processing parameters, interface, and fusion additive. However, the recent researches mostly focused on the effect of processing parameters and bonding mechanism. Almost no investigation has been carried out on the impact of fusion additive. Therefore, the polyphenylene sulfide (PPS) additive having similar molecular structure with the CFRTP matrix was chosen as the fusion additive in the present study. The laser joining of CFRTP and stainless steel with different PPS additive thickness was conducted. The microstructure, interface morphology, and mechanical properties of the CFRTP and stainless steel joint were investigated.

1. Experimental Procedures. In the present study, the CFRTP panels with PPS matrix reinforced by T700 carbon fibers were cut into the size of $50 \times 30 \times 3$ mm. The CFRTP is composed by PPS matrix and 15 layers T700 carbon fibers, which is weaved with intersected structure. The carbon fiber is wrapped by the PPS, and the average thickness of the single layer is 0.2 mm. The 304 stainless steel specimens with a size of $50 \times 30 \times 2$ mm were prepared, and their surfaces for laser joining were ground by the 120# abrasive paper to increase the roughness. The chemical composition of 304 stainless steel is given in Table 1.

The joining of stainless steel and CFRTP was conducted by a fiber laser welding system. This system comprises 1410RABB robot, 500 W fiber laser (continuous wave laser machine and the wavelength is 1080 nm), laser processing head (the focal length is 120 mm), air-actuated clamp and cooling system. The schematic diagram of the joining of stainless steel and CFRP by the laser is shown in Fig. 1. Firstly, the CFRTP overlaid with PPS additive on the surface was placed on the laser welding system and the stainless steel plate was placed above the PPS additive. After then, the stainless steel, PPS additive, and CFRTP were clamped by the air-actuated clamp which has a groove with a size of $60 \times 10 \times 5$ mm in the upper one. The clamping pressure could be adjusted by controlling the air-actuator. During the laser joining, the laser beam would scan on the surface of stainless steel in the groove with the argon gas flow velocity of 30 l/min. To investigate the effect of the PPS additive on the joint strength, the thickness of the PPS additive was changed gradually from 0 to 450 μm with the interval of 150 μm. The laser scanning speed, laser power, and clamping pressure were set as 5 mm/s, 320 W, and 0.5 MPa, respectively. The detailed changes in the processing parameter are listed in Table 2. In all laser-joined specimens, the defocusing distance was −20 mm, and the laser beam diameter was 500 μm.

TABLE 2. The Detailed Processing Parameters of Laser Joining Stainless Steel and CFRTP

Specimen	Laser scanning speed (mm/s)	Laser power (W)	Clamping pressure (MPa)	Thickness of PPS (μm)
S1	5	320	0.5	0
S2	5	320	0.5	150
S3	5	320	0.5	300
S4	5	320	0.5	450

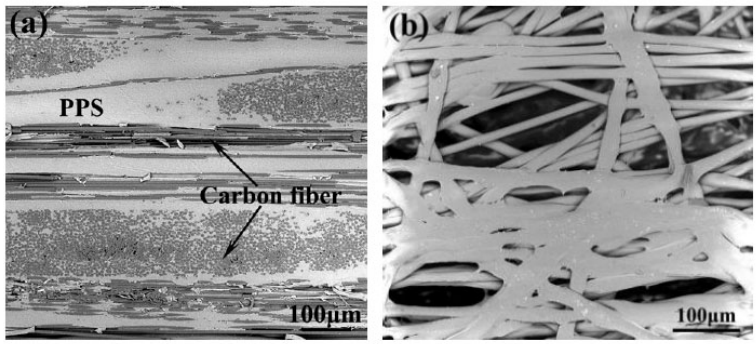

Fig. 2. Morphology of CFRTP with the overlapping of carbon fibers (a) and PPS additive (b).

The microstructure and morphology of PPS additive, CFRTP and stainless steel and CFRTP joint were characterized by the optical microscopy (OM), confocal laser scanning microscope (CLSM), scanning electron microscopy (SEM) and tensile test. The specimen for cross section observation was cut from the stainless steel and CFRTP joint and polished by the conventional metallographic method. The KEYENCE VX-X200 CLSM was employed to analyze the interface of the stainless steel and CFRTP joint. The Phenom Pro SEM was used to observe the microstructure of laser scanned stainless steel and the morphology of joint interface. The tensile test was performed on the UTM4304 electronic universal testing machine to obtain the shear strength. The shear strength test was referred to the GB/T7124-86 and ASTM F2255-2005(2010) standards. The tensile test was carried out in the air with the initial strain rate of $2 \cdot 10^{-3}$ s^{-1} at room temperature. Three specimens of the same condition were tested to obtain the shear strength data. The Stemi 2000 OM was applied to observe the debonding surface of the tensile specimen.

2. Results and Discussion.

2.1. The Microstructure of the CFRTP and PPS Additive. The typical microstructures of PPS based CFRTP and PPS additive are shown in Fig. 2. The PPS based CFRTP is mainly composed of black-grey carbon fiber and white-grey PPS matrix, as shown in Fig. 2a. From the SEM image, it can be found that the carbon fibers are overlapped layer by layer, and most carbon fibers are packed and bonded together by the PPS. Based on the macroscopic observation, the layer of carbon fiber is weaved as decussate structure. The layer of carbon fiber was about 200 μm in thickness, while some layers of higher thickness were also observed. The observation of the layers of carbon fibers revealed that they had the average size of 6 μm in diameter. Moreover, the distribution of PPS in the CFRTP was not uniform, and the interface of the carbon fiber layer preferably coincided with the PPS vacancies, while carbon fibers had good integrity with the regular arrangement. The SEM observation on the PPS additive revealed that the PPS fibers were overlapped randomly, and there was relatively high porosity, as shown in Fig. 2b. Based on the SEM image, the PPS fibers had the average size of 20–30 μm in diameter.

The macro- and micrographs of the laser-joined stainless steel and CFRTP are shown in Fig. 3. The laser scanning results on the stainless steel, which exhibits an apparent oxidation on the track of laser scanning, is shown in Fig. 3a. The observation on the interface of the laser-joined CFRTP and stainless steel reveals that CFRTP has a proper bonding with the stainless steel even without the PPS additive, as shown in Fig. 3b. Such a joined state should be attributed to the existence of PPS in the CFRTP. During the laser joining, the laser scanning on the stainless steel

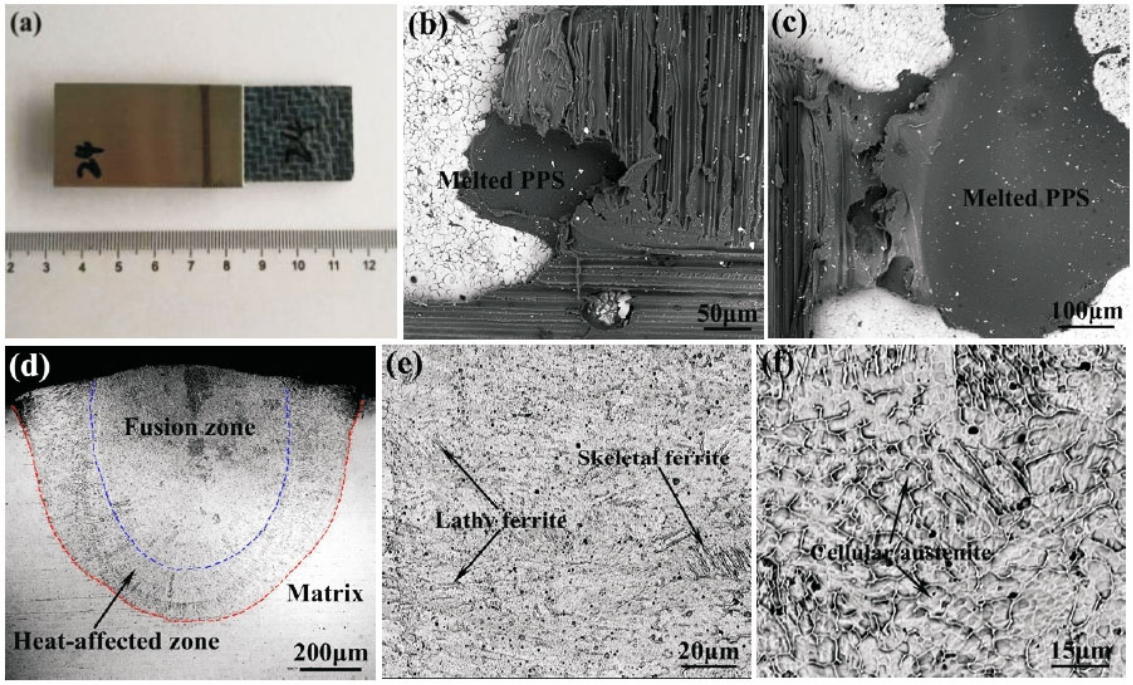

Fig. 3. (a) Macrograph of the laser joined CFRP and stainless steel; (b) morphology of the CFRP on the stainless steel without PPS additive; (c) morphology of the CFRP on the stainless steel with PPS additive; (d) microstructure of the laser-scanned stainless steel; (e) lathy ferrite and skeletal ferrite in the heat-affected zone; (f) skeletal ferrite and cellular austenite in the fusion zone.

would increase the temperature of the steel surface to about 400℃, which could melt the PPS to liquid and spread on the gap of stainless steel and CFRTP [13]. Due to the limited amount of PPS in the CFRTP, the melted PPS could not spread over the gap uniformly. The addition of PPS additive would solve this problem, as shown in Fig. 3c. It can be seen that the molten PPS has filled the gap of steel and CFRTP. Moreover, some molten PPS additive flow get out of the gap and spread over the adjacent stainless steel, but its distribution is not even. The observation on the laser scanned stainless steel revealed that the laser scanning strongly influenced the stainless steel microstructure, as shown in Fig. 3d. There are fusion zone and heat-affect zone (HAZ) in the steel, which have semi-ellipsoidal shapes. In HAZ, the lathy ferrite mainly precipitates along the original grain boundary or twin boundary, which separates the original grain and refines the structure, as shown in Fig. 3e. Moreover, a distinct boundary is formed between HAZ and matrix. With the observation proceeding to the fusion zone, the ferrite becomes coarse and increases, which forms the skeletal structure, as shown in Fig. 3f. There is no distinct boundary between HAZ and the fusion zone. The latter zone is mainly distinguished by the morphology and amount of the ferrite [14]. In the fusion zone, the skeletal ferrite and cellular austenite are the main ingredients. Based on findings [15–18], the higher cooling rate results in the formation of cellular structure. In the present study, a relatively high Cr content and high laser scanning speed are shown to promote the formation of ferrite with intercellular or interdendritic structures.

The shear strength of the stainless steel/CFRTP joints was tested to evaluate the effect of PPS additive on the interface bonding. The shear strength of the stainless steel/CFRTP joints with different PPS share is depicted in Fig. 4. It can be seen that the shear strength of the stainless steel/CFRTP joint without PPS additive is about 7 MPa. A small addition of PPS improves the shear strength of the stainless steel/CFRTP joint, which reaches 9.3 MPa. The shear strength of the stainless steel/CFRTP joint attains the maximum value of 15.1 MPa when the PPS thickness is about 300 μm. Noteworthy is that the shear strength of the stainless steel/CFRTP joint drops significantly to 3.9 MPa, when the PPS thickness is 450 μm. Such variation trend of the shear strength of the stainless steel/CFRTP joint strongly indicates that the PPS additive is instrumental to enhance the adhesive strength between the stainless steel and CFRTP, but its amount should be controlled.

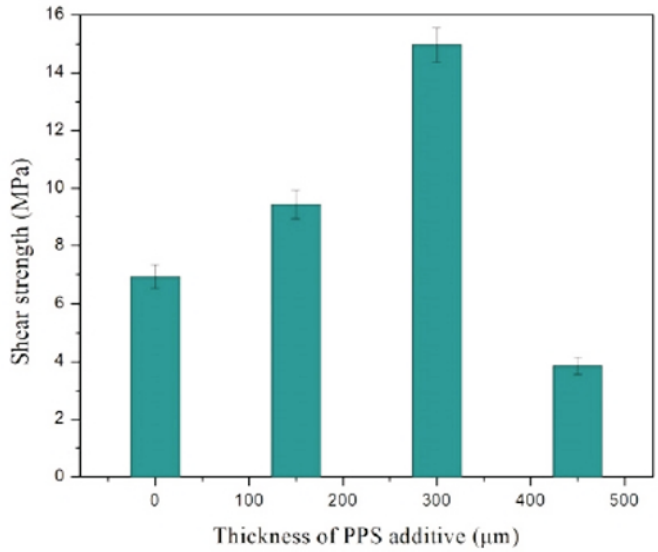

Fig. 4. The shear strength of the stainless steel/CFRTP joints with different thickness of PPS additive.

The observations on the debonding surface of the stainless steel/CFRTP joints with different thickness of PPS additive are shown in Fig. 5. It can be found that the CFRTP still can be joined with the stainless steel without PPS additive, as shown in Fig. 5a. Due to the woven structure of CFRPT, the distribution of melted PPS over the surface of stainless steel is not homogeneous. Moreover, the decomposition of PPS in CFRTP can be observed on the debonding surface of CFRTP. When the thickness of PPS additive increases to 150 μm, the melted PPS additive attached to the surface of stainless steel is thin, as shown in Fig. 5b. Furthermore, the melted PPS additive fills in the vacancy of the CFRTP surface, but such a thickness of PPS additive is not enough to spread and merge with the PPS matrix of CFRTP thoroughly. Therefore, the joint with 150 μm-thick PPS additive has some fiber exfoliation morphology and a relatively low shear strength. On the debonding surface of stainless steel/CFRTP joint with 300 μm PPS additive, one can observe that PPS additive is melted and adhered to the stainless steel surface perfectly, as shown in Fig. 5c. A layer of carbon fiber is exfoliated from the CFRTP and adhered on the CFRTP uniformly, which suggests the PPS additive has good bonding with the stainless steel. With the thickness of PPS additive increased to 450 μm, it adheres to the stainless steel, but the CFRTP surface has almost no melting features, as shown in Fig. 5d.

As shown in Fig. 6, the observation on the interface of stainless steel/CFRTP joints with different thickness of PPS additive exhibits that any addition of PPS additive would result in the formation of air bubbles. When the thickness of the PPS additive is 150 μm, air bubble are regularly distributed over the joint interface, as shown in Fig. 6a. Based on the recent research [13], the formation of this kind of air bubbles should be ascribed to the decomposition of PPS induced by the excessive heat generation. With the thickness of PPS additive increased to 300 μm, the interface has the residual PPS and a few air bubbles, as shown in Fig. 6b. The reduced decomposition implies that the heat transfer is sufficient for the melting of PPS additive. However, on the interface of joint with 450 μm PPS additive, there are many air bubbles, and they prefer to aggregate, as shown in Fig. 6c. Such a phenomenon should be attributed to the insufficient heat transfer. Due to the increased PPS additive, the transferred heat is insufficient for melting the PPS thoroughly to obtain a good fluidity. The residual air in the interface is not removed, which promotes the formation of aggregated air bubbles.

Based on available findings [19, 20], the joining of the dissimilar materials mainly depends on the initial interface bonding. In the present paper, the initial interface bonding is determined by the PPS, which fuses the CFRTP and stainless steel. However, the PPS state during the laser joining is influenced by the processing parameters and thickness of PPS additive [13]. Given that heat transfer from the laser is controlled in this study, PSS thickness determines the fusion of PPS additive. If the amount of PPS additive is too small, it may be overheated and decomposed, which would hinder the coalescence of stainless steel and CFRTP. If the amount of PPS additive is too high, it would fail to melt thoroughly and fill the gap between stainless steel and CFRTP effectively. Therefore, one

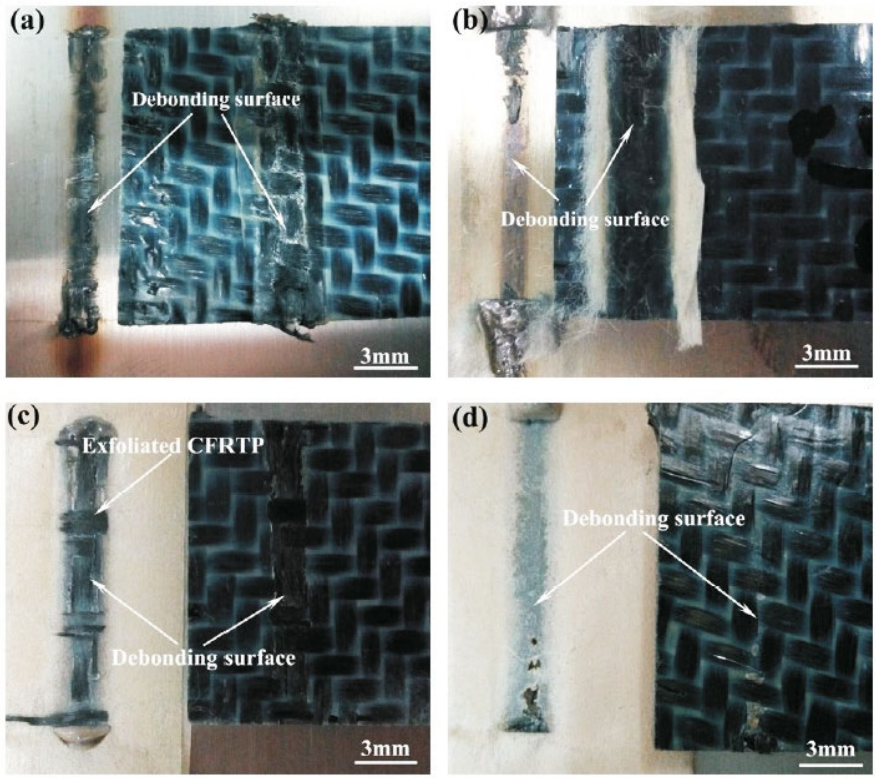

Fig. 5. The morphology of debonding surface of the stainless steel/CFRTP joints with different PPS addition thickness after tensile: (a) 0 μm, (b) 150 μm, (c) 300 μm, and (d) 450 μm.

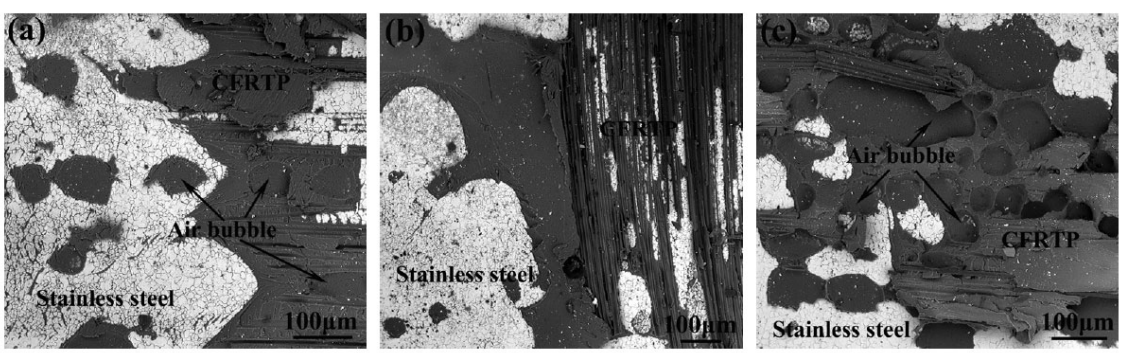

Fig. 6. The interface morphology of the stainless steel/CFRTP joints with different PPS addition thickness: (a) 150 μm, (b) 300 μm, and (c) 450 μm.

can find that there are apparent vacancies or air bubbles in the interface of stainless steel and CFRTP joint with some PPS additive. Thus, the addition of PPS should be controlled, to ensure that it would melt thoroughly and fill the gap between stainless steel and CFRTP. In the present study, the optimal thickness of PPS additive was found to be 300 μm, which corresponded to the best bonding interface and shear strength of stainless steel/CFRTP joint.

CONCLUSIONS

1. CFRTP/304 stainless steel laser joints were produced with and without PPS additive. Without the PPS additive, the PPS in CFRTP could be overheated and decomposed, which is detrimental to the interface bonding. However, the addition of PPS additive was found to improve the CFRTP and stainless steel bonding strength.

2. The laser joining produced the fusion zone and heat-affected zone (HAZ) in stainless steel. In HAZ, the lathy ferrite precipitates along the boundary, which refines the austenite. In the fusion zone, the ferrite forms the skeletal structure and separates the austenite into a small cellular structure.

3. The shear strength of the stainless steel and CFRTP joint can be improved by adding the appropriate amount of PPS additive. Its maximum value of 15.1 MPa was reached when the PPS thickness was 300 μm. Higher or lower PPS thickness values resulted in lower shear strength of the stainless steel/CFRTP joint.

Acknowledgments. The authors are grateful to the support of Shenzhen Basic Research Project (JCYJ20150529162228734, JCYJ20160427100211076, JCYJ20160427170611414, JCYJ20150625155931806, and JCYJ20170306141506805).

REFERENCES

1. A. Pramanik, A. K. Basak, Y. Dong, et al., "Joining of carbon fibre reinforced polymer (CFRP) composites and aluminium alloys – A review," *Compos. Part A-Appl. S.*, **101**, 1–29 (2017).
2. L. Sheng, J. Jiao, B. Du, et al., "Influence of processing parameters on laser direct joining of CFRTP and stainless steel," *Adv. Mater. Sci. Eng.*, **2018**, 2530521 (2018), DOI: 10.1155/2018/2530521.
3. J. Kweon, J. Jung, T. Kim, et al., "Failure of carbon composite-to-aluminum joints with combined mechanical fastening and adhesive bonding," *Compos. Struct.*, **75**, Nos. 1–4, 192–198 (2006).
4. P. Molitor, V. Barron, and T. Young, "Surface treatment of titanium for adhesive bonding to polymer composites: a review," *Int. J. Adhes. Adhes.*, **21**, No. 2, 129–136 (2001).
5. F. Lambiase and D. C. Ko, "Two-steps clinching of aluminum and Carbon Fiber Reinforced Polymer sheets," *Compos. Struct.*, **164**, 180–188 (2016).
6. X. F. Xu, A. Parkinson, P. J. Bates, and G. Zak, "Effect of part thickness, glass fiber and crystallinity on light scattering during laser transmission welding of thermoplastics," *Opt. Laser Technol.*, **75**, No. 6, 123–131 (2015).
7. S. Katayama and Y. Kawahito, "Laser direct joining of metal and plastic," *Scripta Mater.*, **59**, No. 12, 1247–1250 (2008).
8. X. Tan, J. Shan, and J. Ren, "Effects of Cr plating layer on shear strength interface bonding characteristics of mild steel/CFRP joint by laser heating," *Acta Metall. Sin.*, **49**, No. 6, 751–756 (2013).
9. A. Roesner, A. Olowinsky, and A. Gillner, "Long term stability of laser joined plastic metal parts," *Phys. Procedia*, **41**, 169–171 (2013).
10. X. H. Tan, J. Zhang, J. G. Shan, et al., "Characteristics and formation mechanism of porosities in CFRP during laser joining of CFRP and steel," *Compos. Part B-Eng.*, **70**, 35–43 (2015).
11. S. Ridene, "Large optical gain from the 2D-transition metal dichalcogenides of MoS2/WSe2 quantum wells," *Superlattice Microst.*, **114**, 379–385 (2018).
12. J. Jiao, Z. Xu, Q. Wang, et al., "CFRTP and stainless steel laser joining: Thermal defects analysis and joining parameters optimization," *Opt. Laser Technol.*, **103**, 170–176 (2018).
13. J. Jiao, Q. Wang, F. Wang, et al., "Numerical and experimental investigation on joining CFRTP and stainless steel using fiber lasers," *J. Mater. Process. Tech.*, **240**, 362–369 (2017).
14. L. J. Wang, L. Y. Sheng, and C. M. Hong, "Influence of grain boundary carbides on mechanical properties of high nitrogen austenitic stainless steel," *Mater. Design*, **37**, 349–355 (2012).
15. L. Y. Sheng, F. Yang, T. F. Xi, et al., "Microstructure and elevated temperature tensile behaviour of directionally solidified nickel based superalloy," *Mater. Res. Innov.*, **17**, No. S1, 101–106 (2013).
16. L. Y. Sheng, F. Yang, T. F. Xi, et al., "Microstructure evolution and mechanical properties of Ni_3Al/Al_2O_3 composite during self-propagation high-temperature synthesis and hot extrusion," *Mater. Sci. Eng. A*, **555**, 131–138 (2012).
17. L. Y. Sheng, B. N. Du, B. J. Wang, et al., "Hot extrusion effect on the microstructure and mechanical properties of a Mg–Y–Nd–Zr alloy," *Strength Mater.*, **50**, No. 1, 184–192 (2018).

18. L. Y. Sheng, F. Yang, T. F. Xi, et al., "Microstructure and room temperature mechanical properties of NiAl–Cr(Mo)–(Hf, Dy) hypoeutectic alloy prepared by injection casting," *T. Nonferr. Metal. Soc*., **23**, No. 4, 983–990 (2013).
19. F. Lambiase, A. Paolettia, V. Grossi, and S. Genn, "Improving energy efficiency in friction assisted joining of metals and polymers," *J. Mater. Process. Tech*., **250**, 379–389 (2017).
20. L. Y. Sheng, F. Yang, T. F. Xi, et al., "Influence of heat treatment on the interface of Cu/Al bimetal composite fabricated by cold rolling," *Compos. Part B-Eng*., **42**, No. 6, 1468–1473 (2011).